arXiv:1601.05318v1 [cond-mat.supr-con] 20 Jan 2016

Effect of disorder in non-uniform hybrid nanowires with Majorana and fermionic bound states

Zhen-Hua Wang,[1] Eduardo V. Castro,[2] and Hai-Qing Lin[1]

[1] *Beijing Computational Science Research Center, Beijing 100084, China*

[2] *CeFEMA, Instituto Superior Técnico, Universidade de Lisboa, Av. Rovisco Pais, 1049-001 Lisboa, Portugal*

Majorana fermions in some model semiconductor nanowires proximity coupled with s-wave superconductor have been investigated, as well as other intragap bound states in topological phase of a Rashba nanowire with non-uniform spin-orbit interaction (SOI). Using the recursive Green's function method, we present a detailed study of the parameter space for semiconductor-superconductor system focusing on understanding the key experimental conditions required for the realization and detection of Majorana fermions. Various sources of disorder, such as disorder in semiconductor nanowire, bulk superconductor and semiconductor-superconductor interface, are included to characterize their effects on the stability of the topological phase. In the case of multiband semiconducting nanowires, the phase diagram of the system as a function of the chemical potential and magnetic field have been calculated. From the different transverse subbands in the nanowire, a new MF coexisting region appears, where is to a large extent robust against chemical potential fluctuations. In two-band wire or two coupled single band wire, the phase of one band can be controlled through the other band, and these properties is critical to build multiband quantum device. When the SOI vector or magnetic field in semiconductor nanowire rapidly rotates by the angle π, changes its sign, a topological π junction forms at the junction between two wire sections characterized by different directions of the SOI vectors or magnetic field. In this case, some fermionic bound states (FBS) can emerge inside the proximity gap, which localize at the topological π junction, and coexist with Majorana bound states localized at the nanowire ends. Changing the position of the topological π junction from one end to the other, the zero-energy FBS moves and can be used as mediator to transfer quantum information between two distance MFs. Meanwhile, the Andreev spectrum of the junction is qualitatively phase shift by π compared to usual Majorana weak links. The FBS can act as quasiparticle traps and serve as an effective mediator of hybridization between two distant Majorana bound states (MBSs).

PACS numbers: 73.63.Kv, 72.15.Qm, 73.63.Fg, 73.23.-b

I. INTRODUCTION

Bound states arising in a variety of condensed matter systems are explored intensively over the last decade. Excitations with non-Abelian statistics, such as Majorana bound states (MBSs),[1–29] fractional fermions,[30–33] and parafermions[34–40] are attractive due to their potential use in topological quantum computation schemes. The simplest non-Abelian excitation is zero-energy MBS, and recent experimental evidence is consistent with the possibility that superconducting nanowires with strong spin-orbit coupling support topological superconductivity and MBSs.[15–18,29] The key to the experimental realization of Majorana fermions in such system is to satisfy a certain set of requirements that ensures the stability of MBSs and how big the effect is for realistic parameters. The challenging task here is to control fluctuations of parameters and suppress effects of disorder in the realistic systems. In multiband nanowires, the stability of the topological nontrivial phase is enhanced due to strong interband mixing, and the system is most robust against chemical potential fluctuations.[41,42] Therefore, it is essential to identify parameter regimes favorable for the existence of Majorana fermions (MFs) in laboratory, in particular, in the presence of various disorder types and multiband occupancy.

The quantum information encoded in the degenerate states of MBSs is topologically protected from local sources of decoherence. Braiding of non-Abelian anyons have been implemented using one-dimensional semiconductor nanowires, in particular T-junction wire network. Recently, Flensberg *et al.* have demonstrated the non-Abelian rotations in hybrid topological-spin qubit systems, and coherently transfer quantum information between topological qubits and normal spin qubits.[43–46] Also, a composite system of Majorana-hosted semiconductor nanowire and superconducting flux qubits has been shown to process quantum information.[47,48] As is known, MBSs do not have the structure necessary to construct a universal quantum computer. Several methods have been suggested to achieve universal operation, including merging the quasiparticles for a certain time[49] or combining topological and conventional qubits.[47,50,51] Moreover, there are many other intragap bound states in realistic system, such that MBSs can be transformed from fractional fermions by tuning parameters from the topological trivial phase to nontrivial phase.[14] With non-uniform spin-orbit interaction, topological π Josephson junction can support three topological phases protected by chiral symmetry.[52] However, the bound states coexisting with MBSs in some types of topological π Josephson junction has not received much attention, as well as its implications for topological quantum computation. It

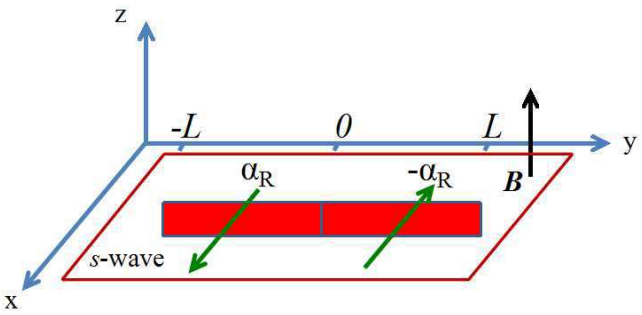

FIG. 1. Sketch of a non-uniform nanowire of length $2L$ on an s-wave superconductor directed along y direction which consists of two segments $y < 0$ and $y > 0$ in which the corresponding SOI vectors α_R and $-\alpha_R$, point in opposite directions. The magnetic field **B** applied perpendicular to the surface can induce a topological regime, where bound states are formed inside the gap. Firstly, there are zero-energy Majorana bound states localized at the nanowire ends $y = \pm L$. Secondly, there are zero-energy fermionic bound states at the interface $y = 0$, where the SOI vector changes its sign.

is still an open question whether other intragap bound states coexisting with MBSs could be used to braid Majoranas, even for universal quantum computing.

The goal of the present work is to develop the recursive Green's function method for the realization and observation of the emergent Majorana mode and other intragap bound states in some model nanowire systems, and discuss the requirements of the stability of MBSs in the presence of various disorder. The multiband nanowires can enhance the topological nontrivial phase and are better suited for observing the Majorana particle. Understanding the property of multiband quantum device is critical to build topological 2D quantum device. With non-uniform spin-orbit interaction and magnetic field, the FBSs can emerge in the topological phase of a Rashba nanowire in the presence of proximity-induced superconductivity gap. Such FBSs can act as quasiparticle traps and thus can have implications for quantum information transfer. Specially, the Andreev spectrum is qualitatively phase shift by π compared to usual Majorana weak links. With even number of topological junction in one wire, there is no phase shift on the Andreev spectrum. At T-junction, by tuning the direction of SOI vector among the three segments, the three MFs at the junction combine into a zero-energy Majorana mode and a finite-energy fermion.

II. MODEL

The physical system for studying Majorana fermions includes a strongly spin-orbit coupled semiconductor, proximity-coupled to an s-wave superconductor and imposed to a Zeeman field. To analyze the robustness of the MBS signature in the real physical system, the single MBS is replaced by the whole nanowire. The sketch is shown in Fig. 1. The continuous BdG Hamiltonian for the system is[5–7]

$$H = \int dy \Psi_\sigma^+ [(\frac{p^2}{2m} - \mu)\delta_{\sigma\sigma'} + 2\alpha_R p \sigma^x_{\sigma\sigma'} - V_z \sigma^z_{\sigma\sigma'}]\Psi_{\sigma'} + i \int dy \Delta \Psi_\sigma^+ \frac{\sigma^y_{\sigma\sigma'}}{2} \Psi^+_{\sigma'} + h.c. \ , \quad (1)$$

where μ is chemical potential, the indices $\sigma, \sigma' = \uparrow, \downarrow$ represent the spin direction. $\Psi_\sigma(y)$ annihilates spin-σ electrons at position y, $\sigma^z_{\sigma\sigma'}(\sigma^x_{\sigma\sigma'}, \sigma^y_{\sigma\sigma'})$ are Pauli matrices.

For numerical convenience, it is standard to study the BdG equation in a discrete lattice tight-binding approximation with no loss of generality and with fewer unknown parameters. Under the lattice approximation, we can map Eq. (1) to a tight-binding model:

$$H_{wire} = H_0 + H_{Rashba} + H_Z + H_{SC} \ , \quad (2)$$

where H_0 includes nearest-neighbor hopping along the wire (y direction),

$$H_0 = \sum_{i,\sigma} [-t(w^+_{i+1,\sigma} w_{i,\sigma} + w^+_{i,\sigma} w_{i+1,\sigma}) - \mu_{LAT} w^+_{i,\sigma} w_{i,\sigma}], \quad (3)$$

where $w^+_{i,\sigma}$ creates an electron with spin index σ on site i of the wire. The free electron energy in the lattice model is $\varepsilon_k = -2t \cos k - \mu_{LAT}$, the band width is $4t$. μ_{LAT} is the chemical potential of the wire in the lattice model. The band has a energy $-2t$ shift compared to the continuum Hamiltonian $\varepsilon_k = \frac{k^2}{2m} - \mu$. So, the chemical potential in this two model are not the same, they must satisfy the relation $\mu_{LAT} = \mu - 2t$. The Rashba spin-orbit interaction can be written as,

$$H_{Rashba} = \sum_{i,\sigma\sigma'} -i\alpha_R w^+_{i+1,\sigma} \sigma^y_{\sigma\sigma'} w_{i,\sigma'} + h.c. \ . \quad (4)$$

The direction of α_R determines the direction in which the spins are polarized by the SOI. In the case of non-uniform SOI, without loss of generality, we choose α_R to be positive for $y < 0$, and negative for $y > 0$. A magnetic field is applied perpendicular to the surface (z direction) causing the Zeeman splitting V_Z,

$$H_Z = \sum_i V_Z (w^+_{i\uparrow} w_{i\uparrow} - w^+_{i\downarrow} w_{i\downarrow}). \quad (5)$$

The s-wave pairing term with superconducting order parameter Δ is

$$H_{SC} = \Delta \sum_i (w^+_{i\uparrow} w^+_{i\downarrow} + w_{i\downarrow} w_{i\uparrow}) \ . \quad (6)$$

To account for the spin-flip due to spin-orbit coupling and the superconducting pair potential, we make use of the 4×4 spin⊗Nambu space,[53–55] spanned by $\Psi_i = (w^+_{i\uparrow}, w^+_{i\downarrow}, w_{i\uparrow}, w_{i\downarrow})^T$. The matrices of the nanowire for $i = 1, 2, ...N$ are

$$H_{ii}=\begin{pmatrix} -\mu_{LAT}+V_Z & 0 & 0 & \Delta \\ 0 & -\mu_{LAT}-V_Z & -\Delta & 0 \\ 0 & -\Delta & \mu_{LAT}-V_Z & 0 \\ \Delta & 0 & 0 & \mu_{LAT}+V_Z \end{pmatrix},\ H_{i,i+1}=\begin{pmatrix} -t & -\alpha_R & 0 & 0 \\ \alpha_R & -t & 0 & 0 \\ 0 & 0 & t & \alpha_R \\ 0 & 0 & -\alpha_R & t \end{pmatrix}=(H_{i+1,i})^+ . \tag{7}$$

For a small system size, the full tight-binding model can be analyzed directly by exact diagonalization. However, for sufficiently large system, exact diagonalization is not realizable. We will solve the BdG equation by a recursive Green's function method.

In a more realistic system, a critical ingredient for realizing Majorana fermions in a solid state hybrid system is the proximity-induced superconductivity. To address quantitative aspects of the SC proximity effects, one has to consider specific models for the relevant terms in the total Hamiltonian:[56,57]

$$H_{tot}=H_{SM}+H_{Rashba}+H_Z+H_{SC}+H_{SM-SC},$$

$$H_{SC}=\sum_{i,j,m}(t_{ij}^{sc}-\mu_{sc}\delta_{i,j})a_{im}^+a_{jm}+\Delta_0\sum_i(a_{i\uparrow}^+a_{i\downarrow}^++a_{i\downarrow}a_{i\uparrow}),$$

$$H_{SM-SC}=\sum_{i_0,j_0}\sum_{m,\sigma}[\tilde{t}_{i_0j_0}^{\sigma m}w_{i_0\sigma}^+a_{j_0m}+h.c.], \tag{8}$$

where H_{SC} describes s-wave bulk superconductor and H_{SM-SC} represents the SM-SC coupling. μ_{sc} is the chemical potential at the SC surface, a_{im}^+ is the creation operator corresponding to state with spin m localized near sites i, $\tilde{t}_{i_0j_0}^{\sigma m}$ are coupling matrix elements between SM and SC local states. In this case, the SM system is embedded into an extended system by applying a self-energy term, Σ_{SC}. Applying the Dyson equation allows us to simplify $G_{tot}=(E-H_{SM}-\Sigma_{SC})^{-1}$, where the self-energy term is given by $\Sigma_{SC}=V_{SM-SC}G_{SC}V_{SM-SC}^+$, and V_{SM-SC} is the coupling between SM-SC. Using the recursive Green's function method similar to Fig. 8, the Green function of the extended two-dimensional superconductor surface can be calculated,[58,59] and then we can obtain the self-energy term Σ_{SC}.

Recent works have also demonstrated that Majorana end states can be realized outside the strict one-dimensional limit.[10,41,42,56,60] Here we consider a quasi-one-dimensional system where the topological phase emerges from different transverse subbands in the nanowire. An effective two-band model for the semiconductor nanowire is constructed, and the Hamiltonian of the two decoupled bands are similar to Eq. (3)-(5):

$$\begin{aligned} H_0=&\sum_{i,s}[-t(w_{i+1,s}^+w_{i,s}+w_{i,s}^+w_{i+1,s})-\mu_{LAT}w_{i,s}^+w_{i,s}] \\ &+\sum_i V_Z(w_{i\uparrow}^+w_{i\uparrow}-w_{i\downarrow}^+w_{i\downarrow})+\sum_{i,s}[-t(d_{i+1,s}^+d_{i,s} \\ &+d_{i,s}^+d_{i+1,s})-(\mu_{LAT}-E_{sb})d_{i,s}^+d_{i,s}] \\ &+\sum_i V_Z(d_{i\uparrow}^+d_{i\uparrow}-d_{i\downarrow}^+d_{i\downarrow}) \end{aligned} \tag{9}$$

$$\begin{aligned} H_{Rashba}&=\sum_{i,ss'}-i\alpha_Rw_{i+1,s}^+\sigma_{ss'}^yw_{i,s'}+h.c. \\ H_{Rashba}&=\sum_{i,ss'}-i\alpha_Rd_{i+1,s}^+\sigma_{ss'}^yd_{i,s'}+h.c. \end{aligned} \tag{10}$$

The spin-orbit band-mixing Hamiltonian reads as:[41,42]

$$H_{SO}^{(12)}=\sum_{i,ss'}E_{bm}[w_{i,s}^+(i\sigma_x)d_{i,s'}-d_{i,s}^+(i\sigma_x)w_{i,s}]. \tag{11}$$

The multiband proximity-induced SC can be described as

$$\begin{aligned} H_{SC}=\sum_i[&\Delta_{11}w_{i\uparrow}^+w_{i\downarrow}^++\Delta_{22}d_{i\uparrow}^+d_{i\downarrow}^+ + \\ &\Delta_{12}w_{i\uparrow}^+d_{i\downarrow}^++\Delta_{21}d_{i\uparrow}^+w_{i\downarrow}^++h.c.]. \end{aligned} \tag{12}$$

Here $w_{i,s}$ and $d_{i,s}$ represent fermion annihilation operators of the first and second subbands. Assuming that the confinement energy along the x direction E_{sb} is larger than all the relevant energy scales of the Hamiltonian. E_{bm} is the band mixing energy, and the multiband induced SC pairing potential Δ_{ij} depend on the microscopic details of the SM-SC interface.

III. RESULTS AND DISCUSSION

A. Effect of disorder in uniform nanowire

Single-channel semiconductor nanowire have been recently proposed as a possible platform for realizing and observing Majorana physics in solid-state systems.[5,6,56] To obtain better insight into the existence of Majorana fermion and other intragap bound states, together with various types of disorder in the realistic system, we calculate the local density of states (LDOS), energy spectrum and electron wave function for several relevant regimes, using a set of control parameters.

1. Disorder in uniform nanowire

For a clean nanowire, the clear-cut evidence for the existence of the Majorana zero modes can be obtained by driving the system from trivial phase to topological nontrivial phase. In the topological trivial phase there is a well-defined gap for all excitations, including states localized near the ends of the wire. By contrast, the topological nontrivial phase is characterized by sharp zero-energy peaks localized near the ends of the wire and separated from all other excitations by a well-defined minigap. In

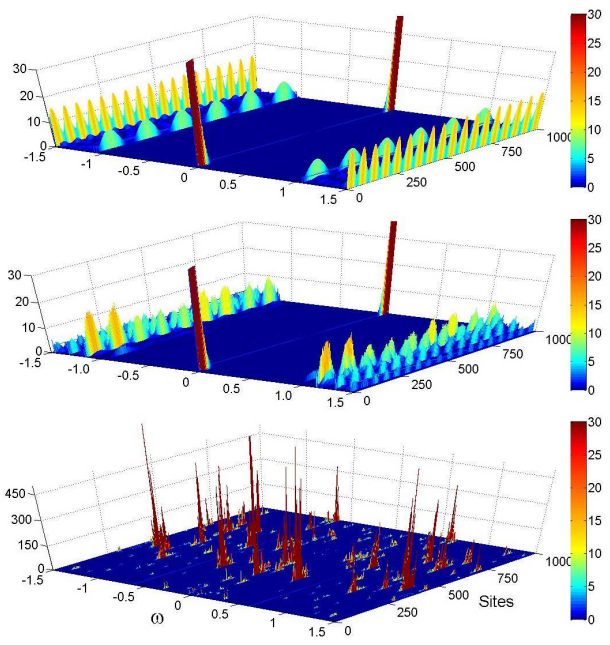

FIG. 2. LDOS for a uniform nanowire with disorder. The strength of the disorder is $r = 0$ (top), $r = 1$ (middle), and $r = 8$ (bottom). Notice that all the low-energy states are strongly localized, but the clear-cut distinction between two phases holds at weak disorder. Throughout, $\mu = 0$, $\Delta = 1.0$, $\alpha_R = 10$ and $V_z = 3.0$, the hopping in the nanowire $t = 10$ corresponds to a band width $D = 40$, and the wire consists of 1000 sites.

both phases, the LDOS is always symmetric, with the DOS at positive energy being exactly the same as for negative energy and also exactly the same at both ends of the wire.

Disorder in the nanowire can have significant adverse effects on the stability of the topological nontrivial phase.[56,61–63] In a realistic system, disorder comes in various ways that affect the topological phase very differently. In this paper we consider three types of disorder: Disorder in the SM wire, impurities in the s-wave SC, and random nonuniform coupling between the SM wire and the SC. For disorder in the SM wire, we focus on the sources that are the most relevant experimentally: random potentials created by charged impurities. We model the random potential by adding to the Hamiltonian the term

$$H_{disorder} = \sum_i V_i c_i^+ c_i \ , \tag{13}$$

where the random set $\{V_i\}$ is normally distributed with zero mean and standard deviation $\{r\}$. We use $\{r\}$ to control the disorder strength. Fig. 2 shows a segment of the LDOS as a function of lattice sites and energy ω for typical disorder realizations at three disorder strengths. For weak to moderate disorder strength, the Majorana zero mode survives, and the main effects of

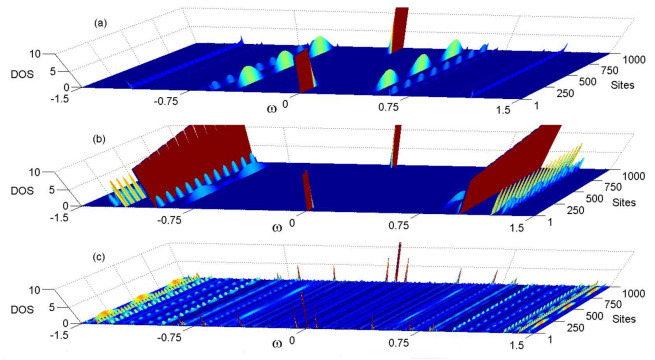

FIG. 3. The LDOS of the semiconductor nanowire proximity on a s-wave superconducting surface for various parameters. (a) The SM-SC coupling $\tilde{t}^{\sigma m}_{i_0 j_0} = 2$, and Zeeman field on the SC surface $V_Z^{SC} = 0$, (b) $\tilde{t}^{\sigma m}_{i_0 j_0} = 3$, $V_Z^{SC} = 0$, and (c) $\tilde{t}^{\sigma m}_{i_0 j_0} = 3$, $V_Z^{SC} = 3$. Other parameters: $\mu_{SC} = 0, t^{sc}_{ij} = 10, \Delta_0 = 3, \tilde{t}^{\sigma m}_{i_0 j_0} = 2, \mu_{SM} = -20, \alpha_R = 10, t = 10$.

disorder are to narrow the spectral gap to the lowest excited states, and to break the parity degeneracy of the excited states.[64] In contrast with the clean case, all the low-energy excitations are strongly localized. However, for sufficiently strong disorder, the excitation gap closes and the Majorana modes no longer exist. Adding disorder induces localization, and the topological non-trivial phase transforms into trivial phase, which is characterized by the closing of the gap[65–67] and by a spectral weight distributed over a wide energy range. Meanwhile, the disorder in the Rashba and Zeeman terms are also an effective way of closing the topological gap. These results are in good agreement with those obtained in Ref. [56]. We have also crosschecked results using the recursion method[68] and obtained perfect agreement.

2. *Proximity-induced superconductivity*

Using the recursive Green's function method, the proximity-induced superconductivity for realizing Majorana fermions in a solid state hybrid system can be investigated. We can now include the superconductor surface self-energy Σ_{SC} into the semiconductor nanowire Hamiltonian and realize the Majorana zero-mode. Fig. 3 shows the LDOS of the SM nanowire for various parameters in the SC surface, including SM-SC coupling $\tilde{t}^{\sigma m}_{i_0 j_0}$ and Zeeman field V_Z. The obtained result is consistent with previous work.[56] At low energies ($\omega \ll \Delta_0$), the frequency dependence of the dynamically generated terms in the self-energy can be neglected, and the effective proximity gap is independent of ω. With the increase of $\tilde{t}^{\sigma m}_{i_0 j_0}$, the self energy Σ_{SC} increases, and the strong coupling make it would require extremely high magnetic fields to reach the topologically nontrivial phase. In the bottom figure of Fig. 3, both SM and SC are considered to be under the same Zeeman field V_Z, which is possible under exper-

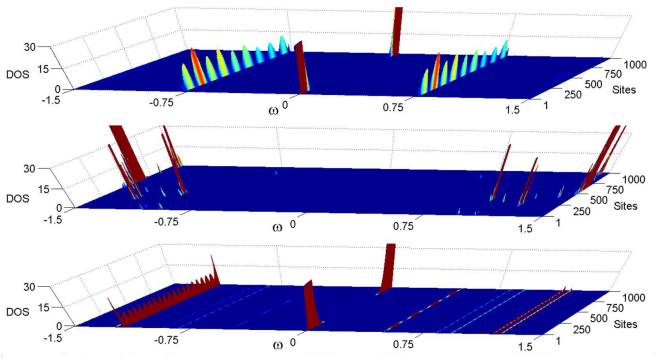

FIG. 4. LDOS of the SM-SC system in the presence of disorder. (a)-(b) Disorder from SC-SM coupling, $\tilde{t} = \tilde{t}^{\sigma m}_{i_0 j_0} + \Delta\tilde{t}$, (a) $r = \Delta\tilde{t}$, (b) $r = 5\Delta\tilde{t}$, where $\{\Delta\tilde{t}\}$ are normally distributed. (c) Disorder from SC surface with $r = 1$. The signature features of the topological nontrivial phase are preserved for weak or mediate disorder.

imental condition. It is found that the gap closes and the Majorana zero-mode disappears. That may be one reason why it's difficult to observe MF in experiment, and this condition should be avoided.

3. *Random nonuniform SM-SC coupling and impurities in the s-wave SC*

Moreover, suppressing effects of disorder and controlling fluctuations of other parameters are challenging tasks. The disorder in SM wire has been discussed above, and we will investigate the other two types of disorder. Firstly, we discuss the disorder in SM-SC coupling, $\tilde{t} = \tilde{t}^{\sigma m}_{i_0 j_0} + \Delta\tilde{t}$, where $\Delta\tilde{t}$ represents the random component. As can be seen from Fig. 4, the signature features of the topological nontrivial phase are preserved for weak or mediate disorder. This is consistent with Ref. [Bena]. Strong disorder induce the disappearance of the zero Majorana modes, and the spectral gets localized. Similar phenomenon can be observed in the presence of nonuniform SC surface, $H_{disorder} = \sum_i V_i a^+_{im} a_{im}$, where $\{V_i\}$ are normally distributed. Therefore, any other significant type of disorder generates the same LDOS behavior, and does not change the key property of Majorana bound states before reach a certain size.

4. *Multiband semiconductor nanowire*

In this part, the Majorana end states are discussed outside the strict one-dimensional limit. Fig. 5 shows the phase diagram for the two-band nanowire model as a function of the chemical potential μ and external magnetic field V_Z. The emergent region of Majorana modes in the system and the corresponding phase diagram are obtained by using local tunneling. Tunneling of electrons to the ends of the nanowire would reveal a pronounced zero-bias peak, in particular, it is e^2/h in the topological nontrivial phase, $G_{peak} = 1/2$, in contrast to that for a dot coupled to a regular fermionic zero mode, $G_{peak} = 0$, and its topologically trivial phase, $G_{peak} = 1$.[55,69,70] In Fig. 5(a), when the confinement energy and spin-orbit band mixing energy $E_{sb} = E_{bm} = 0$, the two bands decouple and Majorana fermions emerge from different transverse subbands at same regions ($|V_Z| > \sqrt{\Delta_{11}^2 + \mu^2}$), which is similar to two physically different chains. However, the much strong Zeeman field ($|V_Z| \gg \sqrt{\Delta_{11}^2 + \mu^2}$) generates a transition from topological nontrivial phase to trivial phase. The blue $R1$ region corresponds to nontopologi-

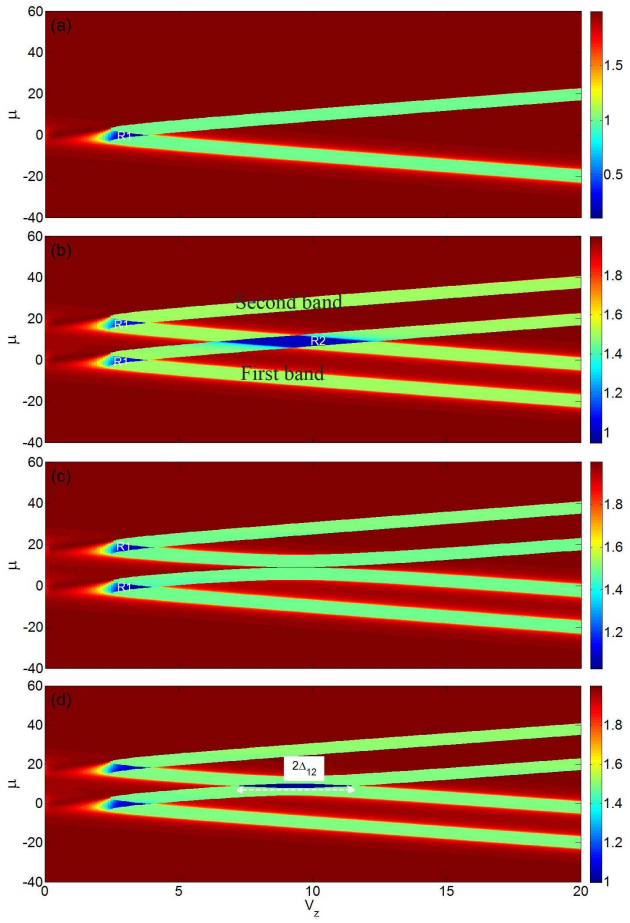

FIG. 5. Phase diagram for the two-band nanowire model as a function of the chemical potential μ and external magnetic field V_z. The pronounced zero-bias peak of detecting quantum dot is used to verify the phase, $A(\omega) = -2\Gamma Im(G^R_{1\downarrow\downarrow}(\omega) + G^R_{2\downarrow\downarrow}(\omega))$. Only the spin-down channel is considered because of the large Zeeman splitting. Realistic parameters of the system are used, we assume here $m^* = 0.04m_e$ with m_e being electron mass and $\alpha = 0.1eV\mathring{A}$ yielding $m^*\alpha^2 \approx 0.6K$. $\tilde{t} = 2.5$, $\tilde{\Delta}_{11} = \tilde{\Delta}_{22} = 4$. (a) $\tilde{E}_{sb} = \tilde{E}_{bm} = \tilde{\Delta}_{12} = \tilde{\Delta}_{21} = 0$, (b) $\tilde{E}_{sb} = 30$, $\tilde{E}_{bm} = \tilde{\Delta}_{12} = \tilde{\Delta}_{21} = 0$, (c) $\tilde{E}_{sb} = 30$, $\tilde{E}_{bm} = 5$, $\tilde{\Delta}_{12} = \tilde{\Delta}_{21} = 0$, (d) $\tilde{E}_{sb} = 30$, $\tilde{E}_{bm} = 5$, $\tilde{\Delta}_{12} = \tilde{\Delta}_{21} = 4$.

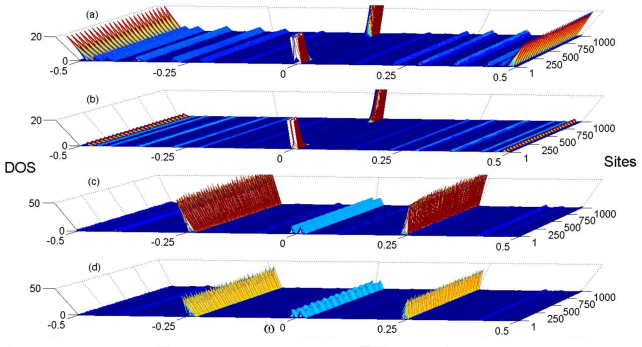

FIG. 6. The LDOS of band 1 (a,c) and band 2 (b,d) in two band nanowire. (a)-(b) $\alpha_{R1} = 0.167, \alpha_{R2} = 0, V_{Z1} = 8, V_{Z2} = 0$. (a)-(b) $\alpha_{R1} = 0.167, \alpha_{R2} = -0.167, V_{Z1} = 8, V_{Z2} = 8$. Other parameters are the same as in Fig. 5(d).

cal phase, $G_{peak} = 0$. With the increase of E_{sb}, see Fig. 5(b), the confinement energy is switched on, and Majorana fermions of two subbands emerge inside different regions ($|V_Z| > \sqrt{\Delta_{11}^2 + \mu^2}, |V_Z| > \sqrt{\Delta_{22}^2 + (E_{sb} - \mu)^2}$). Five distinct phases can be observed, nontopological ($R1$ region), topological trivial phase (red region), topological nontrivial phase with Majorana fermions originating either from first or second subband, and the last one with two Majorana modes localized on each end ($R2$ region). In Fig. 5(c), the spin-orbit band mixing energy E_{bm} modifies the phase boundary. The most interesting parameter regimes is $\mu \sim E_{sb}/2$, two subbands are in topological trivial phase, and two topological nontrivial phases of subbands can't coexist. In the presence of strong interband mixing Δ_{12}, as shown in Fig. 5(d), there is a new window where topological phases from different subbands coexist. At $\mu = E_{sb}/2$ the width of the topologically nontrivial region is given by $E_{sb}/2 - \Delta_{12} < |V_x| < E_{sb}/2 + \Delta_{12}$. The topological phase around this region is to a large extent robust against chemical potential fluctuations, which now have to be $\delta\mu \sim E_{sb}$ to cause the transition into the topological trivial state. This regime provides a promising route to realizing a robust topological nontrivial phase. However, according to our calculation, in this coexisting region, the disorder in the spin-orbit band mixing energy E_{bm} has a sensitive effect on the stability of topological phases. Even for a weak disorder, the topological gap closes and the MF disappears, which is different from other types of disorder in systems. It is therefore required strict conditions to obtain the MF in this region.

Two coupled transverse subbands is similar to two physically different chains. If we change the phase of one band or chain, the other one will also changes. In Fig. 6, the two bands have two sets of control parameters, and we let the two bands be in topological trivial phase firstly ($\alpha_1 = \alpha_2 = 0, V_{Z1} = V_{Z2} = 0$). Then the band 1 is tuned in topological nontrivial phase ($\alpha_{R1} = 0.167, \alpha_{R2} = 0, V_{Z1} = 8, V_{Z2} = 0$), and Fig. 6(a)-(b) corresponds to band 1 and 2. It is found that the band 2 is also in topological nontrivial phase through the spin-orbit band mixing energy E_{bm}. In Fig. 6(c)-(d), the two bands have same parameters except for α_R ($\alpha_{R1} = 0.167, \alpha_{R2} = -0.167$). In this parameter region, the two isolated bands can be in topological nontrivial phase, respectively. But these two bands will be in topological trivial phase when they couple to each other. Therefore, the multiband case or several coupled chains can provide a new way to control the existence of MFs and achieve non-Abelian braiding.

B. Effect of disorder in non-uniform nanowires

1. *Non-uniform Rashba spin-orbit interaction in single band wire*

In this section, we study intragap bound states in the topological phase of a Rashba nanowire with non-uniform spin-orbit interaction and magnetic field. The zero-energy intragap bound states can serve as a mediator to achieve Majorana fermion exchange in strictly one dimensional structures. Firstly, we consider a situation where the SOI vector changes its direction along the nanowire axis creating an interface between two nanowires with different SOI vector directions. The non-uniform nanowire of length $2L$ directed along y direction which consists of two segments, $y < 0$ and $y > 0$ in which the corresponding SOI vectors are in different directions. In the particular case, when the SOI has a sharp discontinuity, such that the SOI vector rapidly rotates by the angle $\phi = \pi$, equivalently, changes its sign, the system possesses an additional symmetry that constrains the fermionic bound states to be zero-energy states. In Fig. 7, we have calculated the LDOS vs ω and lattice sites i for different spin-orbit interaction, including strength and direction. The LDOS symmetries between positive and negative energy is preserved, but which is destroyed at two ends of the wire. The SOI α_R in the top of Fig. 7 have the same direction but with different strength. There are zero-energy Majorana bound states localized at the nanowire ends $y = \pm L$. Having a little change on the strength of SOI does not destroy the signature features of the two phase, and the obtained results are consistent with the discussion of disorder. In the middle figure, $\alpha_R = 10$ for $y < 0$ and $\alpha_R = 0$ for $y > 0$, the half is in topological trivial phase in the region where $\alpha_R = 0$, and the DOS spreads over the entire energy range as there is no finite gap. In the topological nontrivial part, $\alpha_R = 10$, one Majorana zero modes localizes at left end, but the other Majorana zero modes is delocalized and spreads over the $y > 0$ part of the wire. This is due to hybridization of the right hand Majorana with continuum zero energy levels where the gap is closed. In the bottom figure, the two half wire have two α_R with same strength but opposite directions, and additional fermionic bound states emerge inside the proximity gap. They are localized at the junction between two wire sections characterized by different

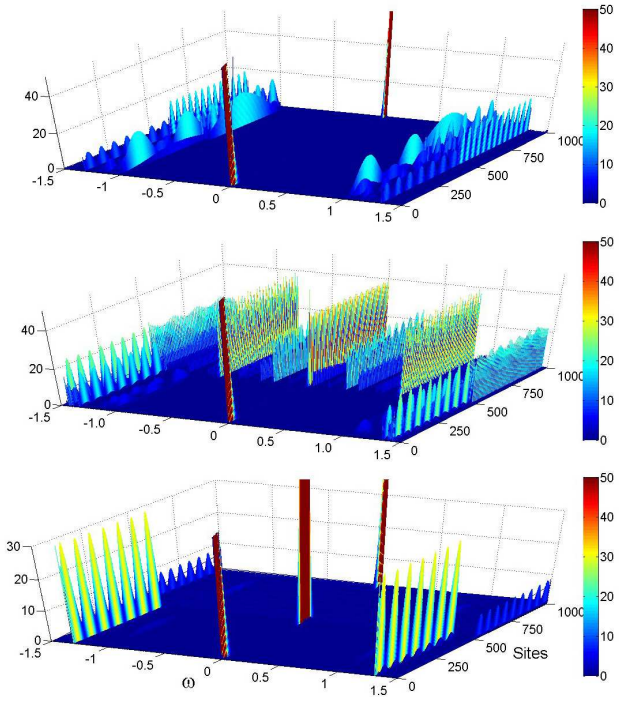

FIG. 7. LDOS for a clean nanowire with non-uniform spin-orbit interaction. For $y < 0$, $\alpha_R = 10$, $y > 0$, $\alpha_R = 5, 0, -10$ from top to bottom,respectively. As the SOI vector changes its sign, the fermionic bound states localize at the interface $x = 0$, coexisting with MBSs at the nanowire ends. Other parameters: $\mu = 0$, $\Delta = 1.0$, $t = 10$ and $V_z = 3.0$.

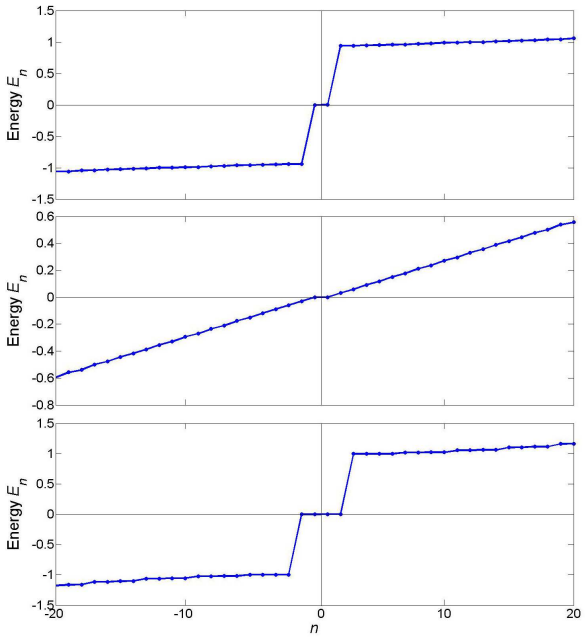

FIG. 8. The energy spectrum for a clean nanowire with non-uniform spin-orbit interaction. The in-gap states are Majorana zero-energy modes, and n labels the eigenvalues of the system with the lowest energy. With opposite SOI vector, the fermionic bound states are zero-energy. Other parameters are the same as in Fig. 7.

directions of the SOI vectors, and they coexist with Majorana bound states localized at the nanowire ends. In the particular case, when SOI change its sign, the FBSs and MBSs are degeneracy since both are zero-energy states.[71]

As discussed above, we only show that the FBS is at the interface in the center of the nanowire. If we change the position of the interface from left to right of the wire, the FBS can serve as a mediator to transfer Majorana fermion, and even exchange MFs in strictly one dimensional structures. The interface is created between two parts with different SOI vector directions, and we let the interface localize at the position of left end of the wire firstly. In this case, the FBS is overlapped with MBS of left end, and there are no FBSs in the gap. Changing the position of the interface from left to right, the information of left MBS can be carried to the right. When the interface localizes at the right end of the wire, the FBS overlaps with the right MBS, and serves as a mediator to transfer information. By fine tuning the parameter, this method even can achieve Majorana fermion exchange in strictly one dimensional structures. Franz *et.al* have demonstrated the MF exchange in 1D structures using π domain wall by tuning the phase of order parameter Δ. The non-uniform Rashba SOI nanowire can also be used to implement protected quantum computation.

To get a deep insight into the additional FBSs, the energy spectrum and electron wave function have been calculated. As shown in Fig. 8, the spectra of uniform nanowire with an odd number of pairs of zero-energy modes characterizes topological SC phases. The in-gap states are Majorana zero-energy modes. When $\alpha_R = 0$, the gap disappears, it is because that the half wire with zero α_R is in topological trivial phase. Therefore, the continuous excitation can cover the entire energy regime. For opposite direction of SOI vector, there are two pairs of zero-energy states in the gap, which are energy degenerate MBSs and FBSs. Note that FBS only exist at zero energy if the angle between SOI vectors is π. For a different angle FBS are not zero energy, and as this angle goes to zero, the states merge in the continuum of excitations.[52,71]

2. *Non-uniform magnetic field*

Next, we replace the uniform magnetic field by non-uniform field. A uniform magnetic field perpendicular to SOI vector can induce a topological phase where MBSs are formed at the ends of the wire. The features illustrated in Fig. 9 are in non-uniform magnetic field. Firstly, we let the magnetic field in the two half wire have same direction but with different strength. The Majorana bound states are also localized at the ends of the

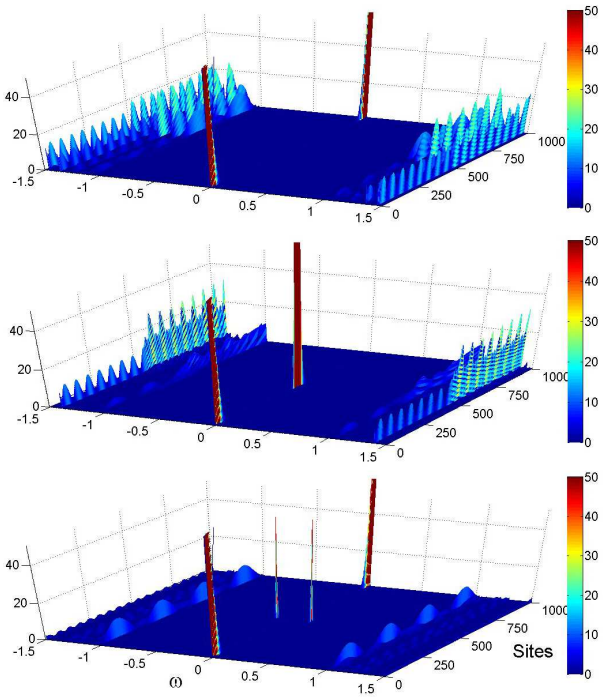

FIG. 9. LDOS for a clean nanowire with non-uniform magnetic field. For $y < 0$, $V_z = 3$, $y > 0$, $V_z = 2, 0, -3$ from top to bottom, respectively. As the magnetic vector changes its sign, the fermionic bound states localize at the interface $y = 0$, coexisting with MBSs at the nanowire ends. $\alpha_R = 10$ and other parameters are the same as in Fig. 7.

wire. As $V_z = 0$ for $y > 0$, there is a gap with no states, since this part of the system is in the non-topological phase. The MBSs localize at the ends of the other half wire for $y < 0$, where the system is in the topological phase. When the two half wire have opposite magnetic field, two additional peaks emerge in the mini-gap, and coexist with the MBSs localizing at the ends of the whole wire. These two peaks have finite energies, which are close to zero-energy. Similar to non-uniform spin-orbit interaction, some intragap bound states emerge in the topological phase. But they are not degenerate with Majorana zero-energy modes.

3. *The effect of disorder on FBSs*

It is also interesting to discuss the effect of disorder on FBSs. Here we only show the disorder of random potentials created by charged impurities in SM nanowire with non-uniform Rashba SOI and zeeman field. Different from the behavior of MBSs in disorder wire, As shown in Fig. 10 (a)-(b), the zero-energy FBS not only coexists with MBS in weak disorder, but also localizes at the interface in strong disorder, where the MBS disappears. In Fig. 10(c)-(e), with the increase of disorder, the non-zero energy FBSs caused by opposite zeeman field run away

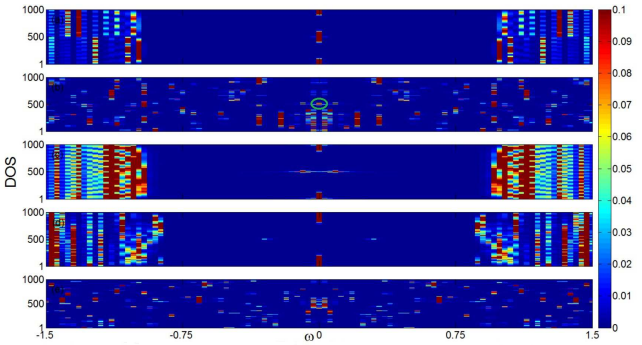

FIG. 10. The LDOS of the non-uniform single band nanowire. (a)-(b) Non-uniform SOI case. The strength of the disorder is $r = 0$ (a), and $r = 8$ (b). Other parameters are in same as Fig. 7. (c)-(e) Non-uniform magnetic field case. The strength of the disorder is $r = 0$ (c), $r = 2$ (d) and $r = 8$ (e). Other parameters are in same as Fig. 9.

from zero-energy and disappear in the continuum excitation states. Therefore, the intragap bound states are more stable than MBSs, and can be serve as an potential way to transfer quantum information.

4. *Double topological junction and T-junction*

Similarly, here we consider a double topological junction composed of two SOI-junction discussed above. In Fig. 11(a)-(b), there are two FBSs localizing at the two junctions. This behavior is very much reminiscent of double quantum dots,[72?] which suggests that such double FBSs can serve as a promising platform for conventional charge qubits. Embedding such charge qubits in a topological superconductor might be rather well protected against environmental noise and thus enjoy unusually large dephasing times. With the increase of topological π junction in the SM nanowire, shown in Fig. 11(c), the zero-energy modes increase. When one dot is connected to two Majorana modes, as shown in Fig. 11(d)-(e), the energetically degenerate states in Flensberg's qubits can be obtained, and through which the two MBSs reduces to a single effective MBS.[43,69] In Fig. 11(d), the semiconductor nanowire has uniform SOI vector, and the energetically degenerate states can be achieved as the phase difference is $\phi = (1 + 2n)\pi$, where ϕ is the magnetic flux through the loop. In Fig. 11(e), non-uniform spin-orbit interaction is used, the behavior of the dot spectrum is nearly the same except for the π phase shift. In this case, only when $\phi = 2n\pi$, the energetically degenerate state in Flensberg's qubit can be obtained. It is because of the topological π junction, changing the sign of the Rashba coupling α_R is effectively equivalent to imposing a rigid phase shift of π to the order parameter. Therefore, the flux qubit in Flensberg's qubit can be canceled out and the hybrid system becomes more controllable and scalable. If there are even number of junction in the wire,

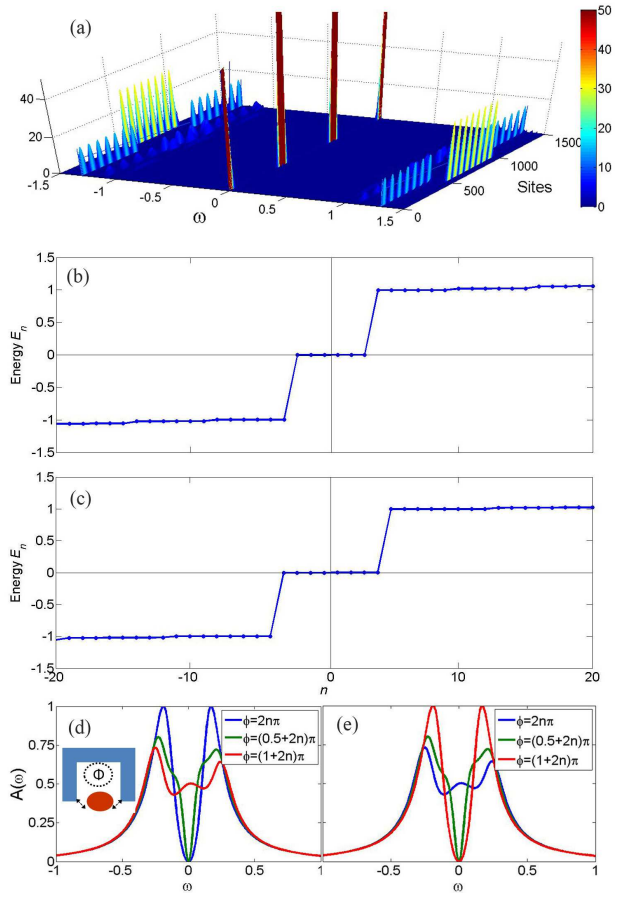

FIG. 11. (a)-(b) The LDOS and energy spectrum for a clean nanowire with a double SOI-junction. (c) Three topological π junction with four pairs zero-energy modes corresponding to one pair MBSs and three FBSs. Other parameters are the same as in Fig. 7. (d)-(e) Dot spectral function in the more realistic nanowire case. (d) Uniform SOI vector, $\alpha_R = 10$, (e) Non-uniform SOI vector, $y < 0$, $\alpha_R = 10$, $y > 0$, $\alpha_R = -10$. The dot spectrum is qualitatively phase shift by π compared to usual Majorana weak links. ϕ are the magnetic flux through the loops, quantum dot level $\varepsilon_d = V_z$, dot-MBS coupling $\Gamma = 0.2$, dot-lead coupling $\lambda = 0.5$.

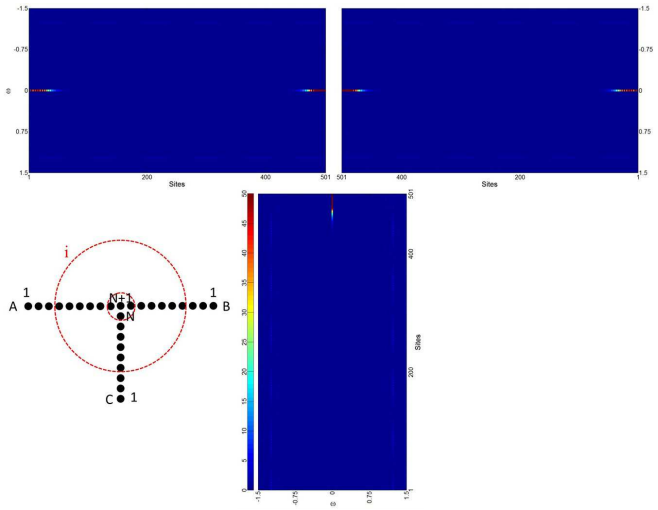

FIG. 12. T-junction viewed as three wire segments with superconducting phases, defined such that the site indices increase upon moving towards the junction, $\Phi_A = \Phi_B = \Phi_C$. Two topological regions with same SOI vector $\alpha_{RA} = \alpha_{RB}$ meeting at the junction form a topological π junction, leading to two pairs MFs existing at the segment ends. Bottom left: Lattice structure giving rise to the T-junction. The recursive Green's function method is used to calculated the LDOS, where i corresponds to a set of ith slice of the T-junction. Other parameters are the same as in Fig. 7.

the phase shift of Andreev spectrum disappears.

A T-junction, three segments meeting at a point, provides the simplest wire network that enables meaningful adiabatic exchange of Majorana fermions.[73] In this part, we'll discuss the intragap bound states at the three segment junction as a function of SOI vector. As Fig. 12 illustrated, the horizontal and vertical wires are taken to consist of $2N + 1$ and N sites, and the phases of every segments are defined such that the site indices increase upon moving towards the junction, $\Phi_A = \Phi_B = \Phi_C$. The recursive Green's function method is used to calculated the LDOS,[58,59] where i corresponds to a set of ith slice of the T-junction. There are three cases to consider that one, two, or three of the wire segments emanating from the junction reside in a topological region. When only one segment is in the topological superconducting state, there are only two MFs and one localizes at the junction. In Fig. 12, two topological segments with same SOI vector, $\alpha_{RA} = \alpha_{RB}$, induce two pairs of MFs emerging, and two MFs exist at the junction, where forming a π junction. It is also interesting to note that there is zero-energy states in vertical wire, although it is in non-topological phase. The reason is that the vertical wire forms π junction between two horizontal wires. But as $\alpha_{RA} = -\alpha_{RB}$, two SOI vector with opposite direction, the two segment end MFs at the junction combine into an finite-energy ordinary fermion. Finally, consider the case shown in Fig. 13 where all three segments are topological, there are three pairs of MFs exist at every segment end when $\alpha_{RA} = \alpha_{RB} = \alpha_{RC}$. Tuning the direction of the SOI vector, $\alpha_{RA} = -\alpha_{RB} = \alpha_{RC}$, the T-junction always supports four Majorana zero modes and one ordinary finite-energy fermion, among which one MBS and the ordinary fermion localize at the junction. Here the Hamiltonian of the junction simplifies to $H_{ABC} \propto -iV_{NN+1}\gamma_C(\gamma_B - \gamma_A)$, where V_{NN+1} is the hopping matrix between Nth and $N + 1$th slice, and $\{\gamma\}$ indicates the Majorana fermions in each wire. It follows that the linear combination $(\gamma_A + \gamma_C)/\sqrt{2}$ remains a zero-energy Majorana mode, while γ_B and $(\gamma_A - \gamma_C)/\sqrt{2}$ combined into a finite-energy fermion. It is imperative to avoid generating spurious zero modes at the T-junction as we braid MBSs. In the presence of non-uniform Rashba SOI nanowire, the T-junction can achieve more quantum operation and be-

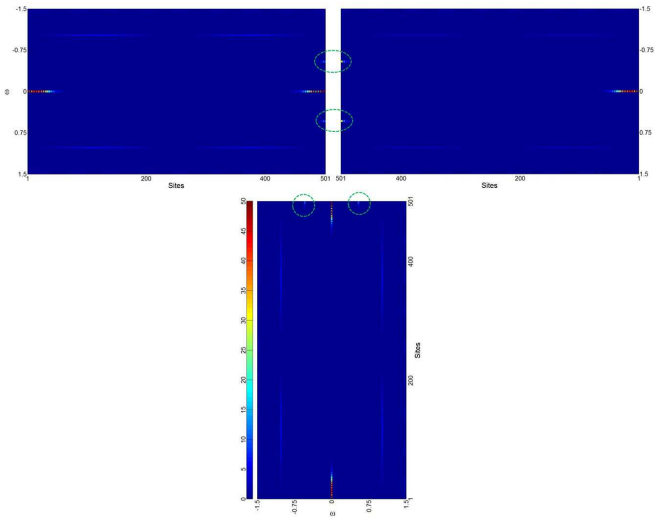

FIG. 13. Three topological segments. when $\alpha_{RA} = -\alpha_{RB} = \alpha_{RC}$, the three Majorana zero modes at the junction combine to form a finite-energy fermion and a single topologically protected Majorana. It follows that the linear combination $(\gamma_A + \gamma_C)/\sqrt{2}$ remains a zero-energy Majorana mode, while γ_B and $(\gamma_A - \gamma_C)/\sqrt{2}$ combined into a finite-energy fermion, corresponding to the peak in the green circles.

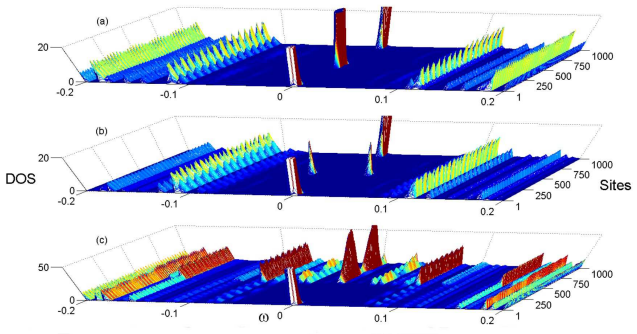

FIG. 14. The total LDOS of the two bands in non-uniform two-band naowire. (a) Both two bands are in non-uniform SOI case. $\alpha_R = 0.167\ (y < 0), \alpha_R = -0.167\ (y > 0), V_Z = 8\ (y < 0), V_Z = 8\ (y > 0)$. (b) Both two bands are in non-uniform magnetic field case. $\alpha_R = 0.167\ (y < 0), \alpha_R = 0.167\ (y > 0), V_Z = 8\ (y < 0), V_Z = -8\ (y > 0)$. (c) Band 1 is uniform but band 2 not, $\alpha_{R2} = 0.167\ (y < 0), \alpha_{R2} = -0.167\ (y > 0), V_{Z2} = 8\ (y < 0), V_{Z2} = -8\ (y > 0)$. Other parameters of the two bands are the same as in Fig. 5(d).

come a potential quantum device.

5. *Non-uniform multiband band nanowire*

The case of non-uniform Rashba SOI and zeeman field is also consider in multiband wire, and the main results are shown in Fig. 14 and 15. Firstly, the two bands have non-uniform Rashba SOI α_R, shown in Fig. 14(a), a pair of zero-energy FBSs appear in the intragap. In

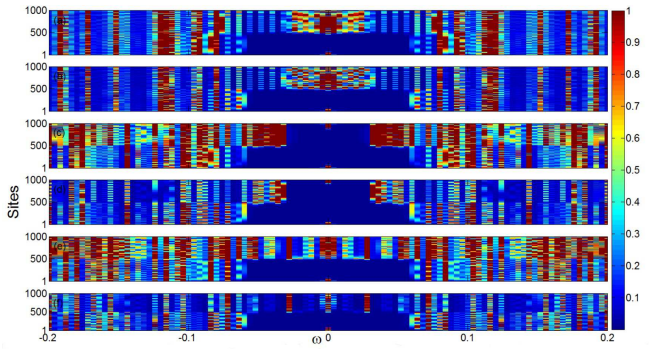

FIG. 15. The LDOS of every bands in the non-uniform two-band naowire, (a,c,e) corresponds to band 1, (b,d,f) corresponds to band 2. (a) Band 1 is uniform, $\alpha_{R1} = 0.167\ (y < 0), \alpha_{R1} = 0.167\ (y > 0), V_{Z1} = 8\ (y < 0), V_{Z1} = 8\ (y > 0)$, band 2 $\alpha_{R2} = 0.167\ (y < 0), \alpha_{R2} = -0.167\ (y > 0), V_{Z2} = 8\ (y < 0), V_{Z2} = 8\ (y > 0)$. (b) $\alpha_{R2} = 0.167\ (y < 0), \alpha_{R2} = 0.167\ (y > 0), V_{Z2} = 8\ (y < 0), V_{Z2} = -8\ (y > 0)$. (c) Both two bands are non-uniform, $\alpha_{R1} = 0.167\ (y < 0), \alpha_{R1} = -0.167\ (y > 0), V_{Z1} = 8\ (y < 0), V_{Z1} = 8\ (y > 0)$ $\alpha_{R2} = 0.167\ (y < 0), \alpha_{R2} = 0.167\ (y > 0), V_{Z2} = 8\ (y < 0), V_{Z2} = -8\ (y > 0)$. Other parameters of the two bands are the same as in Fig. 5(d).

Fig. 14(b), there are two pairs of non-zero energy FBSs in the two band nanowire, whose results are similar to the result in single band. In Fig. 14(c), the band 1 is uniform but band 2 is not, $\alpha_{R2}(y > 0) = -\alpha_{R2}(y < 0), V_{Z2}(y > 0) = -V_{Z2}(y < 0)$, the topological gap in $y > 0$ part is closed, and the right hand Majorana fermion hybridizes with continuum zero energy levels. The behavior of the LDOS is the same as that of Fig. 7, where one half of wire has zero Rashba SOI α_R. This is because that the right parts of the two bands has Rashba SOI with opposite direction, and the effect of opposite α_R is the same as zero Rashba SOI. Therefore, we investigate the case of non-uniform α_R and non-uniform zeeman field in band 2, respectively. It is found that the opposite α_R can close the gap of right part completely, but the opposite zeeman field only narrow the gap. Meanwhile, the intragap bound states hybridize with the continuum excitation states.

IV. SUMMARY AND CONCLUSION

In this paper, we have developed the recursive Green's function method for the realization and the observation of the emergent non-Abelain Majorana mode in some model semiconductor nanowires proximity coupled to an ordinary s-wave superconductor in the presence of various disorder, non-uniform spin-orbit interaction, and non-uniform Zeeman field. Three types of disorder, such as disorder in semiconductor nanowire, bulk superconductor and semiconductor-superconductor interface, are included to characterize their effects on the stability of the

topological phase. It is found that the signature features of the topological SC phase do not depend on the type or the source of disorder. The weak disorder induces strongly localized of the low-energy states, but preserve the signature features. In the topological phase of a Rashba nanowire with non-uniform SOI vector or Zeeman field, the fermionic bound states can emerge inside the proximity gap, localizing at the junction between two wire sections characterized by different directions of the SOI vectors, and they coexist with MBS localized at the nanowire ends. Changing the position of the topological π junction from one end to the other, the zero-energy FBS can be used as mediator to transfer quantum information between two distance MFs, even achieve MF exchange in 1D wire. Specially, the π junction induced fermionic bound states can always exist even for strong disorder, where the topological gap closes. For a double topological junction composed of two SOI-junction, two zero-energy FBSs exist at the two junction, which can hybridize and serve as an effective mediator of hybridization between two distant MBSs. Meanwhile, the Andreev spectrum of nanowire with an odd number of topological junctions is qualitatively phase shift by π compared to usual Majorana weak links. The T-junction provides the simplest wire network that enables meaningful adiabatic exchange of the Majorana fermions. It is imperative that we avoid generating spurious zero-modes to braid MFs at the T-junction. By tuning the direction of SOI vector among the three segments, the three MFs at the junction combine into a zero-energy Majorana mode and a finite-energy fermion. For multiband nanowires, by detecting the spectrum of the coupled quantum dot, we have calculated the phase diagram of the system. The strong interband mixing due to Δ_{12} determines the region where the nontrivial SC states can emerge, and Δ_{12} is crucial for the topological stability of the nontrivial phase. The region is to a large extent robust against chemical potential fluctuations, and this effect is particularly important for experimental realization of Majorana fermions in multiband nanowires. In two-band wire or two coupled single band wire, the phase of one band can be controlled through the other band, and it provides another way to achieve quantum operations. If the two bands are in topological nontrivial phase, but with opposite Rashba SOI, the topological gap will be closed, and MF disappears. These properties is critical for us to build multiband quantum device.

ACKNOWLEDGEMENT

[1] L. Fu and C. L. Kane, Phys. Rev. Lett. **100**, 096407 (2008).
[2] C. Nayak, S. H. Simon, A. Stern, M. Freedman, and S. Das Sarma, Rev. Mod. Phys. **80**, 1083 (2008).
[3] Y. Tanaka, T. Yokoyama, and N. Nagaosa, Phys. Rev. Lett. **103**, 107002 (2009).
[4] M. Sato and S. Fujimoto, Phys. Rev. B **79**, 094504 (2009).
[5] R. M. Lutchyn, J. D. Sau, and S. Das Sarma, Phys. Rev. Lett. **105**, 077001 (2010).
[6] Y. Oreg, G. Refael, and F. von Oppen, Phys. Rev. Lett. **105**, 177002 (2010).
[7] J. Alicea, Phys. Rev. B **81**, 125318 (2010).
[8] M. Z. Hasan and C. L. Kane, Rev. Mod. Phys. **82**, 3045 (2010).
[9] S. Gangadharaiah, B. Braunecker, P. Simon, and D. Loss, Phys. Rev. Lett. **107**, 036801 (2011).
[10] A. C. Potter and P. A. Lee, Phys. Rev. B **83**, 094525 (2011).
[11] J. Klinovaja, S. Gangadharaiah, and D. Loss, Phys. Rev. Lett. **108**, 196804 (2012).
[12] D. Chevallier, D. Sticlet, P. Simon, and C. Bena, Phys. Rev. B **85**, 235307 (2012).
[13] D. Sticlet, C. Bena, and P. Simon, Phys. Rev. Lett. **108**, 096802 (2012).
[14] J. Klinovaja, P. Stano, and D. Loss, Phys. Rev. Lett. **109**, 236801 (2012).
[15] V. Mourik, K. Zuo, S. Frolov, S. Plissard, E. Bakkers, and L. Kouwenhoven, Science **336**, 1003 (2012).
[16] M. Deng, C. Yu, G. Huang, M. Larsson, P. Caroff, and H. Xu, Nano lett. **12**, 6414 (2012).
[17] A. Das, Y. Ronen, Y. Most, Y. Oreg, M. Heiblum, and H. Shtrikman, Nat. Phys. **8**, 887 (2012).
[18] L. P. Rokhinson, X. Liu, and J. K. Furdyna, Nat. Phys. **8**, 795 (2012).
[19] J. R. Williams, A. J. Bestwick, P. Gallagher, S. S. Hong, Y. Cui, A. S. Bleich, J. G. Analytis, I. R. Fisher, and D. Goldhaber-Gordon, Phys. Rev. Lett. **109**, 056803 (2012).
[20] J. Alicea, Rep. Prog. Phys. **75**, 076501 (2012).
[21] M. Leijnse and K. Flensberg, Semicond. Sci. Technol. **27**, 124003 (2012).
[22] S. Nadj-Perge, I. K. Drozdov, B. A. Bernevig, and A. Yazdani, Phys. Rev. B **88**, 020407 (2013).
[23] J. Klinovaja, P. Stano, A. Yazdani, and D. Loss, Phys. Rev. Lett. **111**, 186805 (2013).
[24] B. Braunecker and P. Simon, Phys. Rev. Lett. **111**, 147202 (2013).
[25] M. M. Vazifeh and M. Franz, Phys. Rev. Lett. **111**, 206802 (2013).
[26] H. O. H. Churchill, V. Fatemi, K. Grove-Rasmussen, M. T. Deng, P. Caroff, H. Q. Xu, and C. M. Marcus, Phys. Rev. B **87**, 241401 (2013).
[27] C. Dutreix, M. Guigou, D. Chevallier, and C. Bena, Eur. Phys. J. B **87**, 1 (2014).
[28] K. Pöyhönen, A. Weststrom, J. Röntynen, and T. Ojanen, Phys. Rev. B **89**, 115109 (2014).
[29] S. Nadj-Perge, I. K. Drozdov, J. Li, H. Chen, S. Jeon, J. Seo, A. H. MacDonald, B. A. Bernevig, and A. Yazdani, Science **346**, 602 (2014).
[30] R. Jackiw and C. Rebbi, Phys. Rev. D **13**, 3398 (1976).

[31] S. Gangadharaiah, L. Trifunovic, and D. Loss, Phys. Rev. Lett. **108**, 136803 (2012).
[32] D. Rainis, A. Saha, J. Klinovaja, L. Trifunovic, and D. Loss, Phys. Rev. Lett. **112**, 196803 (2014).
[33] A. Saha, D. Rainis, R. P. Tiwari, and D. Loss, Phys. Rev. B **90**, 035422 (2014).
[34] M. Cheng, Phys. Rev. B **86**, 195126 (2012).
[35] D. J. Clarke, J. Alicea, and K. Shtengel, Nat. commun. **4**, 1348 (2013).
[36] Y. Oreg, E. Sela, and A. Stern, Phys. Rev. B **89**, 115402 (2014).
[37] J. Klinovaja and D. Loss, Phys. Rev. Lett. **112**, 246403 (2014).
[38] E. Sagi and Y. Oreg, Phys. Rev. B **90**, 201102 (2014).
[39] A. Vaezi and M. Barkeshli, Phys. Rev. Lett. **113**, 236804 (2014).
[40] C. P. Orth, R. P. Tiwari, T. Meng, and T. L. Schmidt, Phys. Rev. B **91**, 081406 (2015).
[41] R. M. Lutchyn, T. D. Stanescu, and S. Das Sarma, Phys. Rev. Lett. **106**, 127001 (2011).
[42] R. M. Lutchyn and M. P. A. Fisher, Phys. Rev. B **84**, 214528 (2011).
[43] K. Flensberg, Phys. Rev. Lett. **106**, 090503 (2011).
[44] M. Leijnse and K. Flensberg, Phys. Rev. Lett. **107**, 210502 (2011).
[45] M. Leijnse and K. Flensberg, Phys. Rev. B **86**, 104511 (2012).
[46] M. Leijnse and K. Flensberg, Phys. Rev. B **86**, 134528 (2012).
[47] F. Hassler, A. Akhmerov, C. Hou, and C. Beenakker, New J. Phys. **12**, 125002 (2010).
[48] Z.-T. Zhang and Y. Yu, Phys. Rev. A **87**, 032327 (2013).
[49] S. Bravyi, Phys. Rev. A **73**, 042313 (2006).
[50] L. Jiang, C. L. Kane, and J. Preskill, Phys. Rev. Lett. **106**, 130504 (2011).
[51] P. Bonderson and R. M. Lutchyn, Phys. Rev. Lett. **106**, 130505 (2011).
[52] T. Ojanen, Phys. Rev. B **87**, 100506 (2013).
[53] Z. Y. Zeng, B. Li, and F. Claro, Phys. Rev. B **68**, 115319 (2003).
[54] R. Mélin and S. Peysson, Phys. Rev. B **68**, 174515 (2003).
[55] B. H. Wu and J. C. Cao, Phys. Rev. B **85**, 085415 (2012).
[56] T. D. Stanescu, R. M. Lutchyn, and S. Das Sarma, Phys. Rev. B **84**, 144522 (2011).
[57] T. D. Stanescu and S. Tewari, J. Phys.: Condens. Matter **25**, 233201 (2013).
[58] M. Yamamoto, T. Ohtsuki, and B. Kramer, Phys. Rev. B **72**, 115321 (2005).
[59] M. Settnes, S. R. Power, J. Lin, D. H. Petersen, and A.-P. Jauho, Phys. Rev. B **91**, 125408 (2015).
[60] E. Gaidamauskas, J. Paaske, and K. Flensberg, Phys. Rev. Lett. **112**, 126402 (2014).
[61] A. M. Lobos, R. M. Lutchyn, and S. Das Sarma, Phys. Rev. Lett. **109**, 146403 (2012).
[62] A. R. Akhmerov, J. P. Dahlhaus, F. Hassler, M. Wimmer, and C. W. J. Beenakker, Phys. Rev. Lett. **106**, 057001 (2011).
[63] D. Bagrets and A. Altland, Phys. Rev. Lett. **109**, 227005 (2012).
[64] A. C. Potter and P. A. Lee, Phys. Rev. Lett. **105**, 227003 (2010).
[65] W. DeGottardi, D. Sen, and S. Vishveshwara, Phys. Rev. Lett. **110**, 146404 (2013).
[66] i. d. I. Adagideli, M. Wimmer, and A. Teker, Phys. Rev. B **89**, 144506 (2014).
[67] J. D. Sau and S. Das Sarma, Phys. Rev. B **88**, 064506 (2013).
[68] V. Heine, D. Bullett, R. Haydock, and M. Kelly, "Solid state physics vol. 35, p. 215, edited by h. ehrenreich, f. seitz and d. turnbull," (1980).
[69] D. E. Liu and H. U. Baranger, Phys. Rev. B **84**, 201308 (2011).
[70] Z.-H. Wang, X.-Y. Kuang, M.-M. Zhong, Z.-X. Yang, and H. Li, EPL (Europhys. Lett.) **106**, 67008 (2014).
[71] J. Klinovaja and D. Loss, Eur. Phys. J. B **88**, 1 (2015).
[72] R. Hanson, L. P. Kouwenhoven, J. R. Petta, S. Tarucha, and L. M. K. Vandersypen, Rev. Mod. Phys. **79**, 1217 (2007).
[73] J. Alicea, Y. Oreg, G. Refael, F. von Oppen, and M. P. A. Fisher, Nat. Phys. **7**, 412 (2011).